Cell–cell adhesion accounts for the different orientation of columnar and hepatocytic cell divisions

Francisco Lázaro-Diéguez and Anne Müsch

Department of Developmental and Molecular Biology, Albert Einstein College of Medicine, Bronx, NY

Mitotic spindle alignment with the basal or substrate-contacting domain ensures that dividing epithelial cells remain in the plane of the monolayer. Spindle orientation with respect to the substratum is established in metaphase coincident with maximal cell rounding, which enables unobstructed spindle rotation. Misaligned metaphase spindles are believed to result in divisions in which one daughter loses contact with the basal lamina. Here we describe a rescue mechanism that drives substrate-parallel spindle alignment of quasi-diagonal metaphase spindles in anaphase. It requires a Rho- and E-cadherin adhesion–dependent, substrate-parallel contractile actin belt at the apex that governs anaphase cell flattening. In contrast to monolayered Madin–Darby canine kidney cells, hepatocytic epithelial cells, which typically feature tilted metaphase spindles, lack this anaphase flattening mechanism and as a consequence maintain their spindle tilt through cytokinesis. This results in out-of-monolayer divisions, which we propose contribute to the stratified organization of hepatocyte cords in vivo.

Introduction

The orientation of mitotic cell divisions contributes to how cells arrange within a tissue. Monolayered and stratified epithelia maintain their distinct tissue organization because of a 90° difference in the orientation of their mitotic spindle and hence cell division axis along the cells' *x*-*z* dimension (Ragkousi and Gibson, 2014). In monolayered cells such as those of the kidney or lung, astral microtubules (MTs) are captured in metaphase by cortical cues that are positioned at an equal distance from the basal surface at opposite lateral domains, aligning the metaphase spindle parallel to the basal domain. The cleavage furrow assembles perpendicular to the spindle pole axis, bisecting the luminal surface and thus leading to a symmetric division in which both daughters remain in the plane of the monolayer. This is referred to as planar division (Reinsch and Karsenti, 1994; Tuncay and Ebnet, 2016). In contrast, stratified epithelia such as those of the skin or esophagus undergo orthogonal divisions in which the spindle orients perpendicular and the cleavage furrow forms parallel to the basal surface, resulting in daughters stacked on top of each other. Such divisions also yield nonidentical daughters if the mother cell has apical-basal polarity, as is the case during stratification of the basal layer of the skin (Lechler and Fuchs, 2005; Siller and Doe, 2009; Williams and Fuchs, 2013).

Hepatocytes, the parenchymal cells of the liver, represent a unique third epithelial tissue type. They organize in branched one- or two-cell-wide cords. Like monolayered and unlike stratified epithelia, all hepatocytes within the cords contact lumina and, at their basal surfaces, an endothelium. But unlike monolayered and similar to stratified epithelia, each hepatic cord is multilayered, interspersed with a canalicular luminal network (Gerber and Thung, 1987; Treyer and Müsch, 2013; Gissen and Arias, 2015; Fig. 1 A).

Hepatocytes actively divide during liver development, and cell divisions contribute to liver regeneration after injury in the adult (Miyaoka et al., 2012). How hepatocytes arrange their cell division axis to maintain or acquire the unique liver architecture is incompletely understood. Mitotic profiles in tissue sections of adult livers undergoing regeneration after partial hepatectomy revealed that hepatocytes, unlike monolayered cells, rarely bisect their luminal domain in cytokinesis (Bartles and Hubbard, 1986). This preserves canalicular lumen organization and prevents the generation of acini. The polarized hepatocytic cell lines WIF-B9 and HepG2 mimic this mode of cell division in culture, which is a result of a stereotypic orientation of the spindle pole axis toward the luminal surface in the cells' *x*-*y* dimension (Lázaro-Diéguez et al., 2013; Slim et al., 2013). The *x*-*y* dimension is critical for lumen fate because hepatocytic luminal domains form perpendicular to the basal or substrate-contacting domains at cell–cell contact sites (Fig. 2 A). In contrast, how the hepatocyte spindle is positioned in the *x*-*z* dimension, which determines whether hepatocytes undergo planar divisions like monolayered epithelia or out-of-monolayer divisions that could contribute to stratification or branching of the

Correspondence to Francisco Lázaro-Diéguez: francisco.lazaro-dieguez@einstein.yu.edu; Anne Müsch: anne.muesch@einstein.yu.edu

Abbreviations used: Dox, doxycycline; FRET, Förster resonance energy transfer; KD, knockdown; LGN, leucine-glycine-asparagine repeat protein; MT, microtubule; P-MLC2, phospho-myosin light chain 2; TJ, tight junction; ZO-1, zonula occludens-1.

The Rockefeller University Press
J. Cell Biol. Vol. 216 No. 11 3847–3859
https://doi.org/10.1083/jcb.201608065

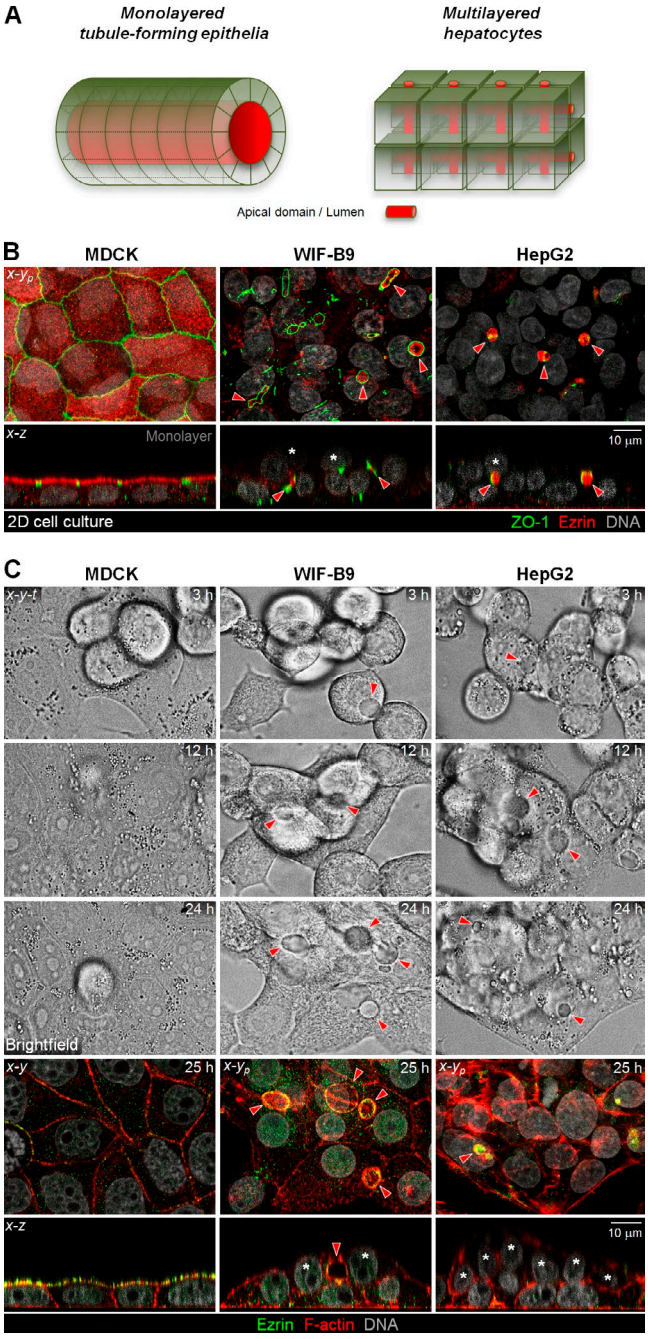

Figure 1. **Hepatocyte-derived cultures form bilayers in two-dimensional cell cultures.** (A) Organization of tubule-forming epithelia and hepatocytes. Lumina are in red. (B) MDCK, WIF-B9 and HepG2 cells grown in 2D cultures were fixed and analyzed for the distribution of the apical protein Ezrin and the TJ marker ZO-1. (C) *x-y-t* brightfield time-lapse sequence of MDCK, WIF-B9, and HepG2 cells plated at equivalent density. Cells were imaged for 25 h, then fixed and stained as indicated. Confocal sections corresponding to the brightfield area (bottom). (B and C) Note the presence of cells not contacting the substratum indicated by asterisks in the nuclei. Arrowheads show hepatocytic lateral lumina.

cords, is not known. We previously observed that WIF-B9 and HepG2 metaphase spindles exhibited not only a stereotypic *x-y* orientation but also a stereotypic oblique angle with the substratum (Lázaro-Diéguez et al., 2013). In this study we sought to establish the consequences of this moderate metaphase spindle tilt: Does it accommodate a substrate-parallel cytokinesis or does it cause divisions in which one daughter becomes detached from the substratum, leading to cell layering?

Whether and under which conditions moderate deviations from substrate-parallel spindle orientation cause out-of-monolayer cell divisions are also important open questions in tubule-forming epithelial cells with defective *x-z* spindle orientation mechanisms. Although it is undisputed that orthogonal spindle positioning leads to aberrant division outcomes (Bergstralh and St Johnston, 2014), geometric rules posit that random spindle orientation in round metaphase cells yields predominantly oblique or near-horizontal spindles (Jüschke et al., 2014). This is borne out in cultured cells where the absence of astral MT-attachment cues causes most spindle pole axes to form shallow or oblique angles with the substratum in metaphase (Toyoshima et al., 2007; den Elzen et al., 2009; Woodard et al., 2010; Kotak et al., 2012; Maier et al., 2013; Jüschke et al., 2014). In these cases the position of the two daughters upon cytokinesis is less clear.

Here we report that monolayered kidney epithelial MDCK cells and hepatocytic WIF-B9 and HepG2 cells handle similar oblique metaphase spindle angles to the substratum differently: columnar MDCK cells correct the misalignment in anaphase and avoid divisions out of the monolayer, whereas hepatocytic cells maintain this spindle tilt throughout mitosis and divide with one daughter detached from the substratum. We elucidated a Rho- and E-cadherin adhesion–dependent mechanism responsible for these differences.

Results

Tilted metaphase spindle orientation in WIF-B9 cells is associated with cell divisions out of the monolayer

In monolayered epithelia and kidney-derived MDCK cells, each epithelial cell contributes its apical domain to a common lumen (Fig. 1, A [monolayered] and B [MDCK]). Hepatocytes, in contrast, form a branched canalicular network, the bile canaliculi (Fig. 1 A, hepatocytes). In the hepatocytic WIF-B9 and HepG2 cell lines, this polarity phenotype is reflected by luminal domains that form between two neighboring cells (Ihrke et al., 1993; Hoekstra et al., 1999; Decaens et al., 2008; Fig. 1 B, red arrowheads). In both polarity phenotypes, a tight junction (TJ) belt flanks the luminal domains (Fig. 1 B, zonula occludens-1 [ZO-1]).

When we analyzed WIF-B9 and HepG2 cell cultures in *x-z* views, we observed that they are partially bilayered (Fig. 1 B, asterisks; and Video 1), a phenomenon that evolved with time in culture (Fig. 1 C) and might reflect the multilayered hepatocyte organization in vivo. In contrast, multilayering was never observed in MDCK cultures (Fig. 1, B and C). We previously reported that unlike MDCK cells, which feature substrate-parallel metaphase spindles (Reinsch and Karsenti, 1994), WIF-B9 and HepG2 metaphase spindles failed to align parallel to the substratum in metaphase (Lázaro-Diéguez et al., 2013). This prompted us to test whether the multilayering in WIF-B9 and HepG2 cell cultures results from out-of-monolayer cell divisions. We determined that both hepatocytic cell types maintained oblique angles of the spindle pole axis with the substratum (Fig. 2 A, defined as β angle) in anaphase (Fig. 2 C). When we analyzed cytokinesis profiles in the *x-z* dimension in fixed WIF-B9 and HepG2 cells (Fig. 2 B and Video 2) and followed

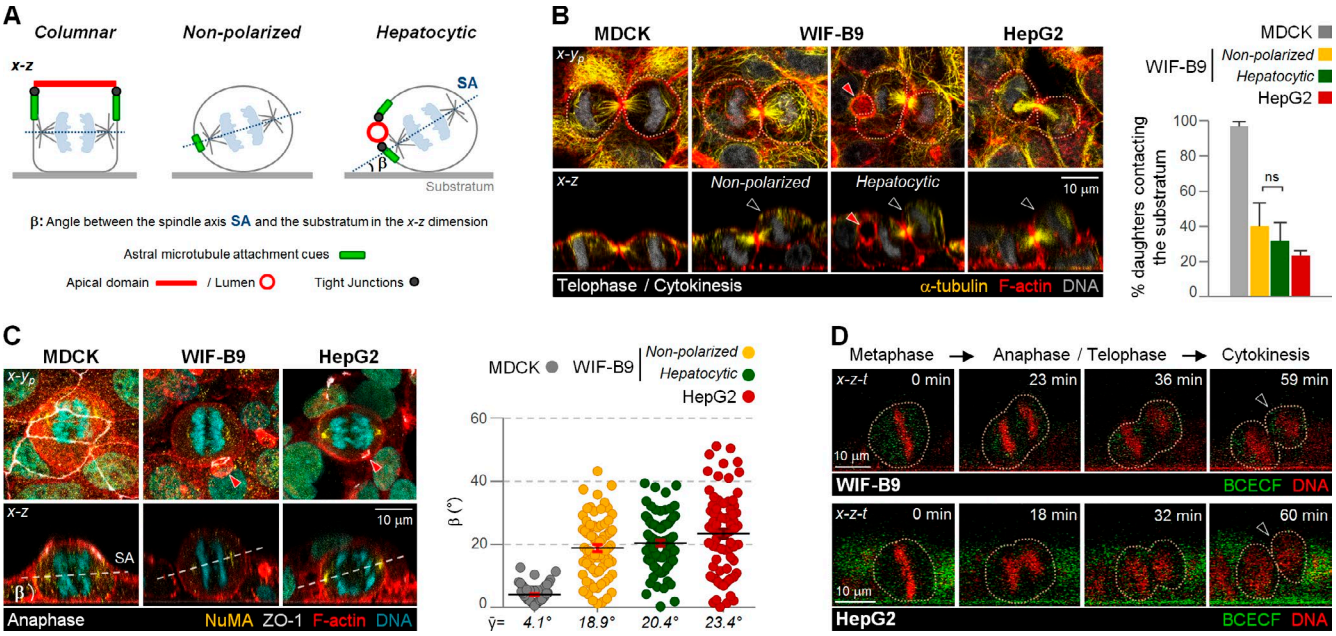

Figure 2. **Hepatocytic cells undergo cell divisions out of the monolayer because of a persistent *x-z* spindle tilt.** (A) Schematics representing the spindle orientation in nonpolarized and columnar- or hepatocytic-polarized anaphase cells. The β angle represents the angle between the spindle axis (SA) and the substratum in the *x-z* dimension. (B and C) MDCK, WIF-B9, and HepG2 cells in late telophase/cytokinesis (B) and anaphase (C) were fixed and stained as indicated. The percentage of cytokinesis with both daughter cells contacting the substratum (B) and the β angle (C) were quantified. n = 20–25 cells/experiment were analyzed for N = 3 independent experiments. ns, not significant, analyzed by t test. Error bars indicate +SD (bar graph) or ±SEM (dot graph). (D) *x-z-t* confocal time-lapse sequence of a dividing WIF-B9 or HepG2 cell with cell contours outlined by pointed lines. (B and C) Red arrowheads show hepatocytic lateral lumina. (B and D) Black arrowheads show daughter that lost substrate contact.

the progression of mitosis in *x-z-t* time lapse (Fig. 2 D), we found that these cells indeed featured tilted cytokinesis profiles, and that one daughter settled on top of a neighboring cell. This was the case regardless of whether the dividing cell contributed to a bile canalicular-like lumen (Fig. 2 B, Hepatocytic, red arrowhead) or lacked a luminal domain (Fig. 2 B, Non-polarized). MDCK monolayers featured, as expected, only substrate-parallel cell divisions (Fig. 2 B). These findings suggest that obliquely tilted mitotic spindles give rise to the bilayered organization of hepatocytic cultures.

Columnar but not hepatocytic polarized cells rescue metaphase spindle tilts in anaphase

To determine whether mitotic spindle tilts also yield out-of-monolayer divisions in other epithelial cell types, we analyzed a MDCK clone knocked down for the astral MT-attachment cue leucine-glycine-asparagine repeat protein (LGN). LGN-knockdown (KD) MDCK cells featured metaphase β angles comparable to those in WIF-B9 cells (Zheng et al., 2010; Fig. S1 C). Yet analysis of cytokinesis profiles in fixed cells (Fig. S1 B) and *x-z-t* imaging of mitotic progressions (Fig. S1 D) revealed that these cells nevertheless divided within the plane of the monolayer and did not multilayer (Fig. S1 A). This was a result of acquisition of a more substrate-parallel spindle orientation (i.e., a decrease in β angle) after progression from metaphase to anaphase (Fig. S1 C). These findings are consistent with previously observed differences between LGN-KD MDCK cells and hepatocytic cells in 3D cultures, where LGN-KD cells arrange in multiluminal cysts (Zheng et al., 2010), whereas hepatocytes (Bell et al., 2016) and HepG2 cells (Kelm et al., 2003) form spheroids without central luminal cavities. We conclude that MDCK cells possess a rescue mechanism for substrate-parallel spindle alignment in anaphase that is lacking in hepatocytic WIF-B9 and HepG2 cells.

To discern if this difference is related to the distinct lumen polarity phenotypes of MDCK and hepatocytic WIF-B9/HepG2 cells, we made use of a MDCK line that inducibly overexpresses the serine/threonine kinase Par1b under a doxycycline (Dox)-repressed promoter (MDCK-Par1b). In MDCK-Par1b cultures, Par1b induction upon removal of Dox (−Dox) causes a switch to hepatocytic polarity with luminal domains interrupting the lateral domain in the majority of cells, whereas a fraction of the cells maintain the native columnar organization of MDCK cells (Fig. 3 A, −Dox; Cohen et al., 2004). We previously reported that both the hepatocytic and the columnar polarized MDCK-Par1b mimicked the metaphase *x-z* spindle orientation of hepatocytic cells (Lázaro-Diéguez et al., 2013; Slim et al., 2013; Fig. 3 C, Metaphase). This allowed us to directly compare putative spindle alignment rescue mechanisms in differently polarized cells of the same cell clone. When we analyzed the cytokinesis profiles of the two populations (hepatocytic and columnar), we observed distinct phenotypes: MDCK-Par1b cells facing a lateral lumen (Fig. 3 B, Hepatocytic) divided with one daughter detached from the substratum, whereas cells without lateral lumen (Fig. 3 B, Columnar) showed similar profiles as control cells (Fig. 3 B, Control, +Dox), in which both daughters remained attached. These differences occur despite comparable spindle tilts in metaphase in the two populations (Fig. 3 C, compare Columnar and Hepatocytic). However, the columnar but not the hepatocytic polarized mitotic MDCK-Par1b cells corrected their spindle alignment with the substratum in anaphase (Fig. 3 C). In support of this rescue, *x-z-t* time-lapse

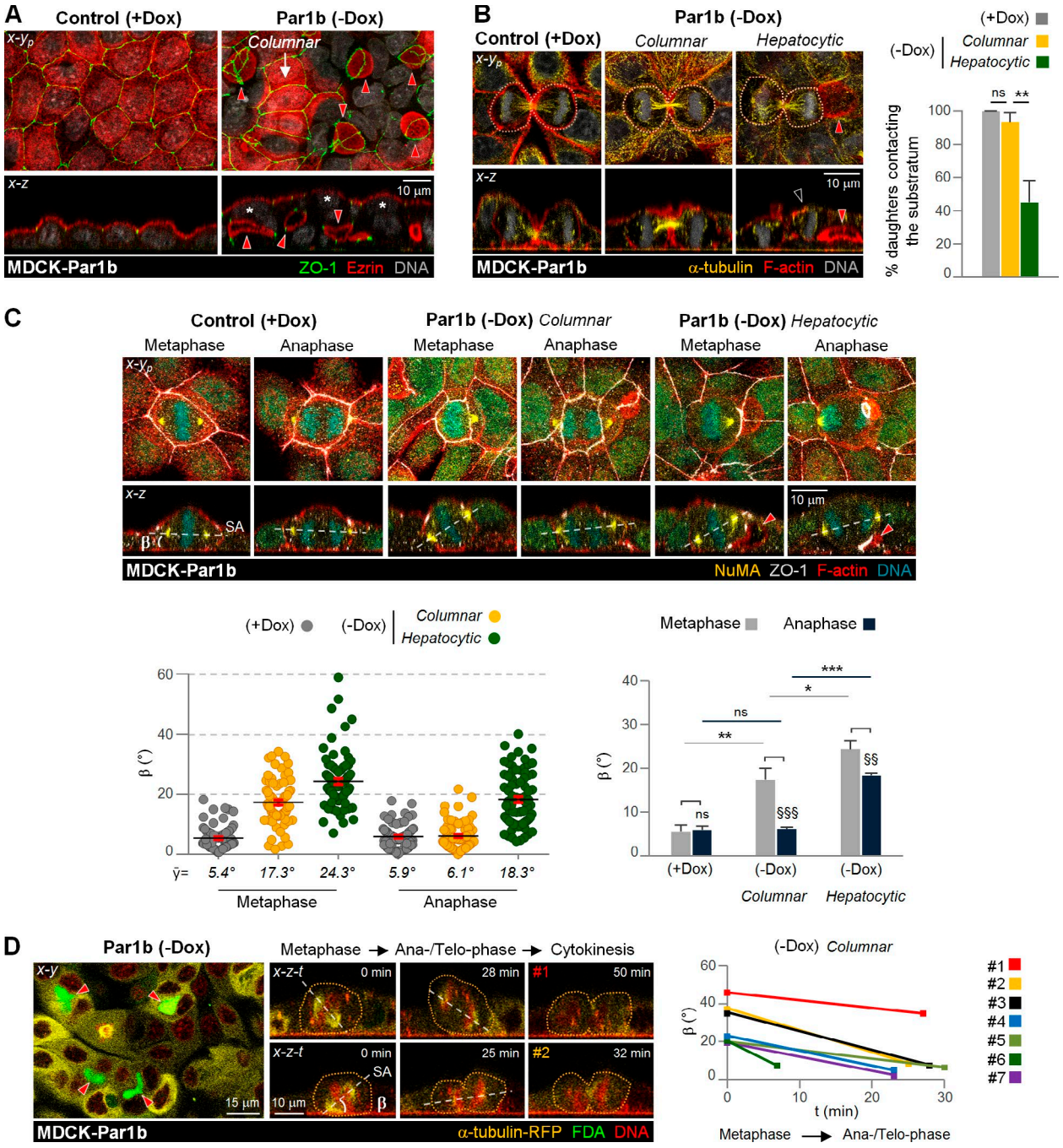

Figure 3. **Tilted metaphase spindle alignment occurs during anaphase in columnar- but not in hepatocytic-polarized Par1b cells.** (A–C) MDCK-Par1b cells uninduced (+Dox) or overexpressing Par1b (−Dox) were fixed and stained as indicated. Asterisks in A and black arrowhead in B indicate nonsubstrate contacting cells and daughters that lost substrate contact, respectively. The percentage of cytokinesis with both daughter cells contacting the substratum (B) and the metaphase and anaphase β angle (C) were quantified. n = 20–25 cells/experiment were analyzed for N = 3 independent experiments. Error bars indicate +SD (bar graphs) or ±SEM (dot graph). *, $P \leq 0.05$; **, $P \leq 0.01$; ***, $P \leq 0.001$; §§, $P \leq 0.01$; §§§, $P \leq 0.001$; ns, not significant, analyzed by *t* test. (D) *x-z-t* Confocal time-lapse sequence of dividing MDCK cells overexpressing Par1b with columnar phenotype. The β angle was followed in seven cells from metaphase to anaphase/telophase profiles. (B and D) Dotted line show cell contours. (A–D) Red arrowheads show hepatocytic-like lateral lumina.

imaging of seven columnar MDCK-Par1b cells showed a consistent decrease in their spindle β angle between metaphase and telophase (Fig. 3 D), although one mitotic cell became substrate-aligned only in cytokinesis (Fig. 3 D, #1).

These findings indicate that the polarity phenotype accounts for the distinct outcomes of mitosis with oblique metaphase spindles in MDCK cells.

Consistent with the prevalence of hepatocytic-polarized cells in the MDCK-Par1b cultures, we also observed substantial multilayering when these cells were allowed to proliferate (Fig. 3 A and Video 3, −Dox). In contrast, multilayering was not apparent when we plated MDCK-Par1b cells at higher confluence and polarized them in calcium switch assays, conditions in which cell divisions are rare (Cohen et al., 2004).

An E-cadherin adhesion-dependent anaphase elongation mechanism that is inefficient in hepatocytic cells

What is the mechanism for the difference in anaphase spindle positioning between cells with columnar and hepatocytic polarity? We noticed that MDCK-Par1b cells with substrate-aligned anaphases (Fig. 3 C and Fig. S2, A and B, +Dox or −Dox Columnar) sported a robust circumferential TJ belt that connected them to all surrounding neighbors as previously reported for MDCK cells (Reinsch and Karsenti, 1994; Fig. S3 A). In contrast, the hepatocytic polarized MDCK-Par1b cells (Fig. 3 C and Fig. S2 B, −Dox Hepatocytic) and WIF-B9 or HepG2 cells that failed to realign the spindle in anaphase either lacked a ZO-1 belt (Fig. S3 B, Non-polarized) or featured a strong ZO-1 belt encircling its lateral lumen but no junctional connection with their other neighbors (Fig. 2 C and Fig. S3 B, Hepatocytic). Analysis of adherens junction markers, which organize TJ assembly, revealed that E-cadherin, p120 catenin, and β-catenin were restricted to cell–cell contacting sites in interphase and throughout all mitotic stages and cytokinesis in MDCK-Par1b cells cultured under +Dox control conditions (Fig. S2 A) and in columnar-polarized cells in −Dox cultures (Fig. S2 B, Columnar). In contrast, adherens junction markers were spread over the entire cell cortex, sparing only the lateral luminal domain in −Dox-cultured MDCK-Par1b cells with hepatocytic polarity (Fig. S2 B, Hepatocytic) and in WIF-B9 cells regardless of their polarity status (Fig. S3). This difference in distribution suggested that hepatocytic cells might cluster E-cadherin and associated catenins less efficiently into zonula adherens, in which E-cadherin is under most tension, linked via its ectodomain to E-cadherin molecules of cell neighbors and via its cytoplasmic domain to a circumferential actin belt (Priya et al., 2015). Indeed, when we compared the fluorescence intensity per surface area, E-cadherin showed significantly weaker labeling of the mitotic cortex in MDCK-Par1b cells compared with the uninduced controls (Fig. 4 A, +Dox vs. −Dox), and hepatocytic-polarized MDCK-Par1b cells featured lower E-cadherin intensity than columnar-polarized cells in the same monolayer (Fig. 4 A, −Dox Columnar vs. Hepatocytic). These observations are consistent with reported higher E-cadherin and catenin staining in monolayered ductal epithelia compared with hepatocytes in the liver (Ihara et al., 1996). To directly compare E-cadherin tension, we employed a previously published MDCK cell line (MDCK-EcadTSMod) expressing a Förster resonance energy transfer (FRET)–based E-cadherin tension sensor, in which an elastic linker, flanked by a mTFP/mEYFP FRET pair, is incorporated between the transmembrane- and β-catenin–binding domains of E-cadherin (Borghi et al., 2012). Tension generated by E-cadherin trans-interactions via its extracellular domain and binding to the actin cytoskeleton via its cytoplasmic domain result in low FRET efficiency, whereas lack of cell–cell adhesion or disruption of microfilaments increases FRET (Borghi et al., 2012). We confirmed these premises using latrunculin B–mediated actin disruption (not depicted) and Rho inhibition (see Fig. 6 F). We then determined that transduction of MDCK-EcadTSMod cells with an adenovirus expressing Par1b increased the FRET efficiency compared with cells transduced with a control adenovirus (Fig. 4 B, CAT), consistent with reduced E-cadherin adhesion in MDCK-Par1b cells.

E-cadherin depletion in MDCK cells was previously reported to cause spindle misalignment with regard to the substratum in both metaphase and anaphase (den Elzen et al., 2009). In an inducible MDCK cell line in which Dox withdrawal leads to the equimolar substitution of endogenous E-cadherin for an adhesion-deficient E-cadherin mutant lacking the extracellular domain (ΔEcad; Troxell et al., 2001) exhibited both multilayering (Fig. 4 C and Video 4, −Dox) and cytokinesis profiles in which one daughter is detached from the substratum (Fig. 4 D). Like the hepatocytic cells, ΔEcad cells failed to correct metaphase-spindle alignment defects in anaphase (Fig. 4 E).

Altogether these data suggest that regardless of the reasons for spindle-alignment deviations in metaphase, E-cadherin tension generated by cell–cell adhesion promotes the correction of shallow spindle tilts in anaphase along with cytokinesis in the plane of the monolayer.

How does E-cadherin–mediated adhesion define the mitotic outcome? We considered two principal mechanisms: (1) adhesion-dependent astral MT attachment cues that actively orient the mitotic spindle in anaphase or (2) adhesion-dependent cell flattening in anaphase that could restrict spindle positioning in the *x-z* dimension in the absence of attachment cues. We ruled out a role for several reported E-cadherin–dependent spindle attachment molecules. They include LGN itself (Gloerich et al., 2017) based on our findings presented in Fig. S1, and adenomatosis polyposis coli protein (den Elzen et al., 2009), because it shows comparable distributions in MDCK and WIF-B9 cells (Rosin-Arbesfeld et al., 2001) and is thus unlikely to be responsible for the different mitotic outcomes between these cell types. We also excluded the E-cadherin binding partner IQGAP1, which has been implicated in an LGN-independent spindle alignment mechanism (Bañón-Rodríguez et al., 2014) as critical for the anaphase rescue of spindle alignment. When we depleted IQGAP1 by RNAi in the LGN-KD cell line (Fig. S4, A and B), no multilayering occurred (Fig. S4 A) and metaphase spindle tilts were still corrected in anaphase in the LGN-IQGAP1-double KD cells (Fig. S4 B).

We therefore considered roles for E-cadherin other than in the organization of cortical spindle attachment complexes. Anaphase transition causes the round metaphase cells to become oblong in their *x-y* dimension to accommodate the separating spindle poles (Cadart et al., 2014). Elongation itself could reduce the β angle independently of astral MT attachment cues if it is associated with cell flattening in the *x-z* dimension. Indeed, we previously observed a nonrandom metaphase spindle positioning in MDCK cells in the absence of cortical cues, which was imposed by the cell cortex that drove spindles longer and/or wider than the cell's height into a tilted quasi-diagonal *x-z* position (Lázaro-Diéguez et al., 2015). So far, only cell-autonomous mechanisms for anaphase elongation have been described, and they considered only the cells' *x-y* dimension (Hickson et al., 2006; Kotadia et al., 2012; Kiyomitsu and Cheeseman, 2013; Rodrigues et al., 2015). We wondered whether E-cadherin–mediated adhesion to cell neighbors contributes to anaphase cell elongation, and whether it involves mitotic cell flattening. To test this hypothesis, we made cell shape comparisons in the MDCK-ΔEcad clone cultured in either +Dox or −Dox. The shape comparisons are based on *x-z* images in which both spindle poles are in focus. They are described by two parameters: 1) a circularity index $C_{x\text{-}z}$, in which 1 represents a circle; and 2) the ratio *h*/*d* of cell height *h* (measured along the axis of the future cleavage furrow) to cell width *d* (measured along the spindle pole axis; Fig. 5 A). We compared cells at a similar anaphase stage, which is defined by the distance *m*

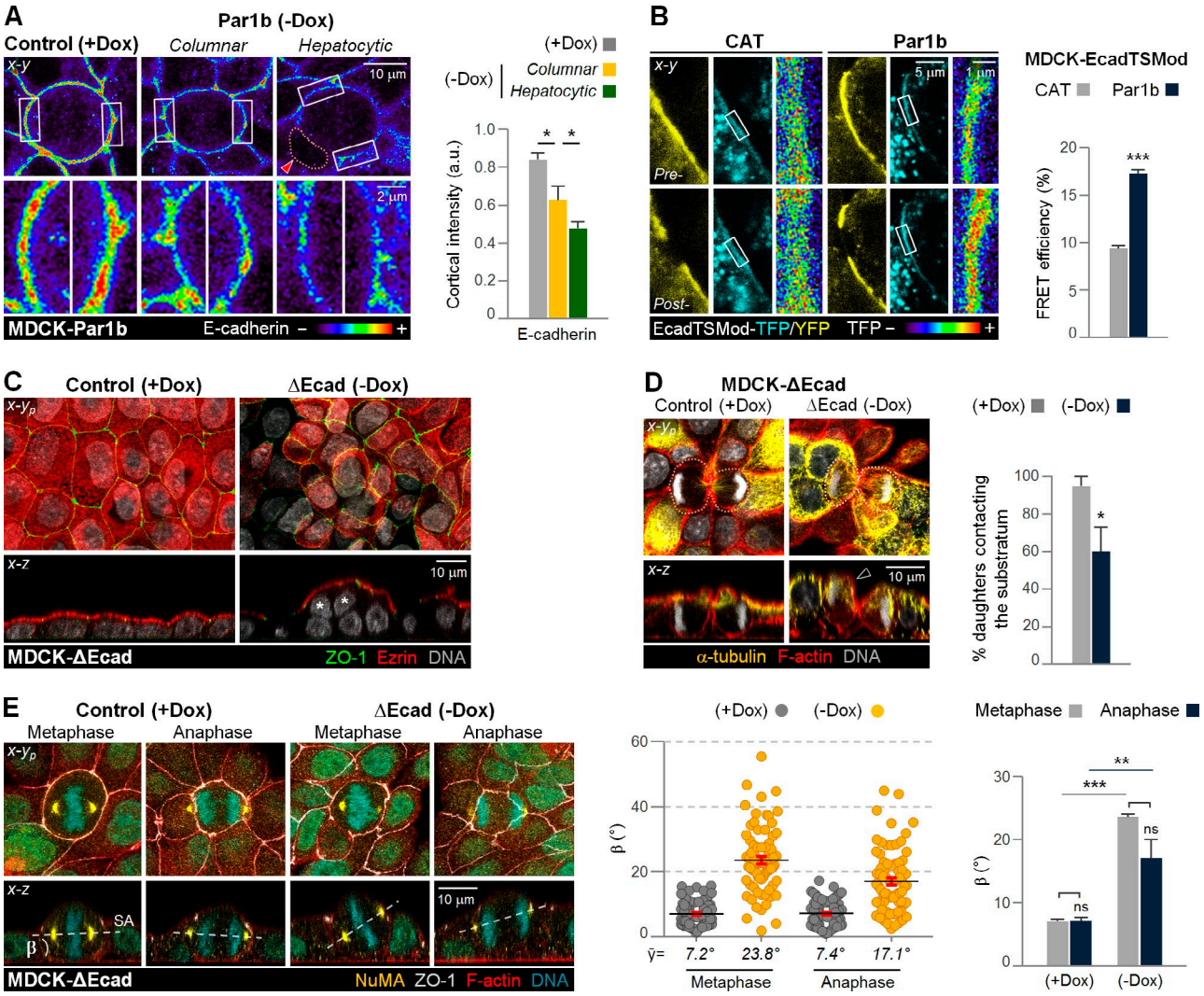

Figure 4. **Anaphase spindle rescue correlates with strong E-cadherin–mediated cell–cell adhesion.** (A) Uninduced control (+Dox) and Par1b–overexpressing (−Dox) MDCK cells were fixed and stained for the adherens junctions proteins E-cadherin, p120 catenin, and β-catenin (see Fig. S2). The intensity of cortical E-cadherin was quantified. Shown are E-cadherin intensity spectrum maps. (Bottom) Enlarged areas of the rectangles in the top panels. Red arrowhead shows hepatocytic-like lateral lumina. (B) FRET efficiency of the E-cadherin tension sensor at cell–cell contacts in control (CAT) or Par1b–expressing MDCK-EcadTSMod cells. Depicted are examples of pre- and postbleach images and the corresponding intensity spectrum maps of the TFP-donor channel. (C–E) Uninduced control (+Dox) and ΔEcad (−Dox) MDCK cells were fixed and stained as indicated. (C) Asterisks indicate nonsubstrate-contacting cells. The percentage of cytokinesis with both daughter cells contacting the substratum (D) and the β angle in metaphase and anaphase profiles (E) were quantified. (D) Dotted lines and black arrowhead represent cell contours and daughter that lost substrate contact, respectively. (A, B, D, and E) n = 20–25 cells/experiment were analyzed for N = 3 independent experiments. Error bars indicate +SD (bar graphs) or ±SEM (dot graph). *, $P \leq 0.05$; **, $P \leq 0.01$; ***, $P \leq 0.001$; ns, not significant, analyzed by t test.

between the separating sister chromatids. −Dox ΔEcad cells exhibited rounder anaphase shapes than their +Dox controls (Fig. 5 B). We also compared MDCK-Par1b cells cultured either under Par1b-induced (−Dox) or uninduced (+Dox) conditions, which represent conditions of low and high E-cadherin tension, respectively. Consistent with the ΔEcad data, −Dox, Par1b-overexpressing cultures featured rounder anaphase cells than the +Dox control cultures (Fig. 5 C). The effect was furthermore dependent on the polarity phenotype: hepatocytic-polarized MDCK-Par1b cells were rounder than the columnar Par1b cells in the same cultures (Fig. 5 C).

Thus, E-cadherin adhesion and E-cadherin tension support anaphase cell flattening. Because the cell shape data correspond well with the differences observed in anaphase spindle alignment, we suggest that cell elongation in anaphase promotes alignment of tilted metaphase spindles parallel to the substratum and a substrate-parallel cytokinesis.

We hypothesized that E-cadherin adhesion promotes the cell shape changes via contractile microfilament bundles at the apical junctional domain, which are well documented in interphase cells (Meng and Takeichi, 2009; Yonemura, 2011). We determined that control MDCK cells featured a strong active myosin II belt in the TJ region (measured by phospho-myosin light chain 2 [P-MLC2] staining) also in anaphase (Fig. 5, D and F, control). Indeed, the P-MLC2 belt exceeded in intensity that of its nonmitotic neighbors to which the mitotic cell is mechanically coupled (Fig. 5 F, control, white and yellow arrowheads, respectively), and it extended with lesser intensity to the entire apex of the anaphase cell. The combined intensity of apical and junctional P-MLC2 was significantly diminished

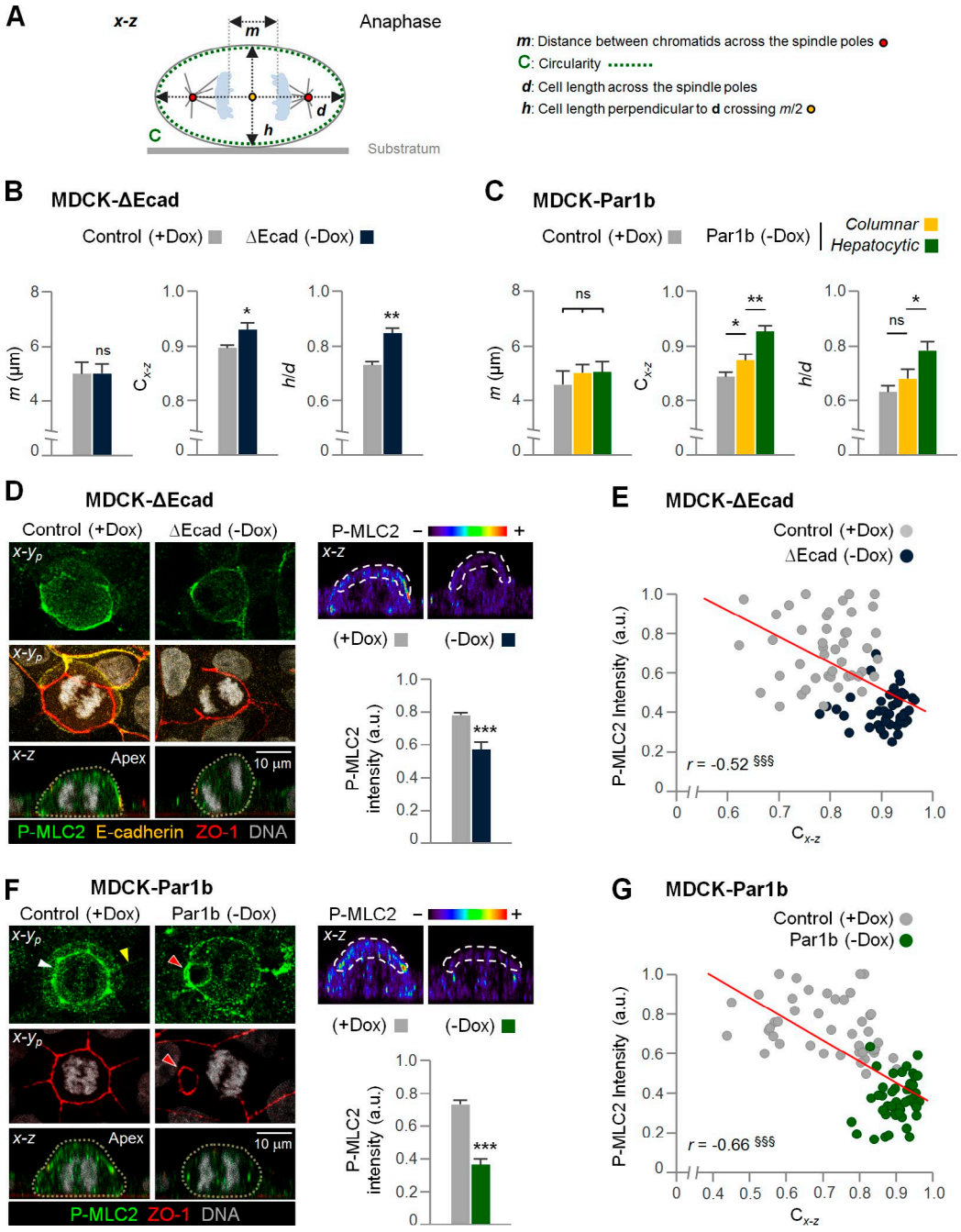

Figure 5. **A contractile junctional adhesion belt is associated with cell flattening in anaphase.** (A) Definition of measured parameters for cell roundness estimation in the *x-z* dimension. (B and C) MDCK-ΔEcad and MDCK-Par1b cells from Fig. 4 E and Fig. 3 C, respectively, were analyzed for *m*, *h*/*d*, and $C_{x\text{-}z}$ values. Note that control cells (+Dox) are less rounded than ΔEcad or Par1b cells (–Dox). *n* = 25 cells/experiment were analyzed for *N* = 3 independent experiments. Error bars indicate +SD. *, P ≤ 0.05; **, P ≤ 0.01; ns, not significant, analyzed by *t* test. (D and F) MDCK-ΔEcad and MDCK-Par1b cells were fixed and stained as indicated. (F) Red arrowhead shows hepatocytic-like lateral lumina. The P-MLC2 intensity spectrum maps for the *x-z* views are shown (right). The intensity of P-MLC2 at the apex (white dashed lines) was quantified. White and yellow arrowheads denote junctional activated myosin II in the mitotic cell and its neighbors, respectively. *n* = 15 cells/experiment were analyzed for *N* = 3 independent experiments. Error bars indicate +SD. ***, P ≤ 0.001, analyzed by *t* test. (E and G) Correlation of anaphase P-MLC2 intensity and $C_{x\text{-}z}$ in control (+Dox) and ΔEcad (E) or Par1b (G) cells (–Dox). §§§, P ≤ 0.001.

when the nonadherent E-cadherin mutant was expressed (Fig. 5 D, compare +Dox- and −Dox-cultured MDCK-ΔEcad cells), confirming that it is dependent on E-cadherin adhesion. Hepatocytic polarized MDCK-Par1b cells, on the other hand, like their control counterparts, featured a strong active subluminal myosin II ring (Fig. 5 F, red arrowheads). However, because of the hepatocytic lumen polarity, the myosin II ring encircled lateral lumina, whereas P-MLC2 intensity at the apex of MDCK-Par1b cells was low (Fig. 5 F). Thus, we tested the idea that it is apical, substrate-parallel myosin activity that corresponds with anaphase flattening. We plotted the apical P-MLC2 intensity against the circularity index $C_{x\text{-}z}$ in individual anaphase cells and found indeed a significant inverted correlation between both parameters, i.e., stronger myosin II at

the cell apex correlated with flatter cells. This was the case for MDCK-ΔEcad cells cultured in +Dox and −Dox (Fig. 5 E) and also for MDCK-Par1b cells (Fig. 5 G).

After P-MLC2 labeling throughout all stages of mitosis (Fig. S5 A), we determined that a contractile actomyosin belt enveloping the entire cortex in metaphase gives rise to mostly apical P-MLC2 in anaphase (Fig. S5 A, *x-z* views for P-MLC2 intensity spectrum map). The horizontal apical contractile belt at the apex could thus conceivably cause an apical constriction and flattening of the anaphase cells. If we assume that the cell maintains a constant volume, the displaced incompressible cytoplasm then exerts isotropic pressure on the cell cortex (Polyakov et al., 2014). This results in the expansion of the cortical regions closest to the separating kinetochores in anaphase cells that are the most elastic (Rodrigues et al., 2015). Thus, we propose that apical constriction by the junctional actin belt acts in conjunction with polar relaxation to mediate anaphase cell elongation in MDCK cells.

To provide additional evidence for this E-cadherin–adhesion and myosin II–dependent spindle rescue mechanism, we sought to manipulate it. Myosin II activity, and E-cadherin adhesion and microfilament incorporation at zonula adherens, mutually reenforce each other through the activities of RhoA and Rho-kinase (Shewan et al., 2005; Priya et al., 2015). If RhoA-dependent myosin II activity is critical for the mitotic outcome, we expect RhoA inhibition in MDCK cells to cause a hepatocytic division and bilayering. We employed a pharmacological Rho inhibitor to test this assumption. As expected, the inhibitor reduced P-MLC2–labeled basal stress fibers and the apical-junctional myosin II ring in interphase cells (Fig. 6 C) and decreased E-cadherin tension as measured by an increase in FRET efficiency of the EcadTSMod biosensor (Fig. 6 F). Similar to our findings with the adhesion-compromised MDCK-ΔEcad and MDCK-Par1b cells, Rho inhibition led to tilted anaphase spindles (Fig. 6 G). It also diminished the apical horizontal myosin II ring in anaphase (Fig. 6 D and Fig. S5 B), which was accompanied by rounder anaphase cells (Fig. 6 H). Finally, Rho inhibition decreased the percentage of both substrate-parallel cytokinesis profiles (Fig. 6 E) and substrate-contacting cells (Fig. 6, A–C, *x-z*, asterisks; and Video 5) as expected if tilted cell divisions lead to multilayering. Rho inhibition thus perfectly phenocopied the cell division phenotype caused by reduced E-cadherin adhesion in MDCK cells. Remarkably, Rho inhibition also promoted hepatocytic lumen polarity (Fig. 6, A and C), in agreement with our prior observation upon RhoA KD (Lázaro-Diéguez et al., 2013), suggesting that the lumen polarity and division phenotypes are intimately linked.

We observed the converse effect on all cell division aspects when we treated WIF-B9 cells with a pharmacological Rho activator. The activator led to strong circumferential junctional P-MLC2–labeling that encircled interphase (Fig. 7 C) and anaphase cells (Fig. 7 D). This was associated with an increase in E-cadherin tension as measured by lower FRET efficiency of the tension sensor (Fig. 7 F). Rho-activated anaphase cells were flatter (Fig. 7 H) and presented with less tilted anaphase profiles (Fig. 7 G) and more substrate-aligned cytokinesis profiles (Fig. 7 E) than the control WIF-B9 cells. In support of a role for the hepatocytic cell divisions in multilayering, Rho-activated WIF-B9 cells were significantly less multilayered (Fig. 7, A–C; and Video 6). Remarkably, Rho-activated WIF-B9 cells adopted the lumen polarity phenotype of columnar monolayered epithelial cells, characterized by a horizontal, "chickenwire-like" TJ organization and a luminal domain at the apex (Fig. 7 A).

These findings support a model in which the substrate-parallel subapical acto-myosin ring associated with the apical junctional complex in columnar but not in hepatocytic polarized epithelial cells enforces anaphase cell flattening and horizontal spindle positioning. Further, our data show that Rho activity links the epithelial lumen positioning and cell division phenotypes. The precise mechanisms for the interdependence of both features are subject for future studies, in which we will test the hypothesis that weak RhoA-dependent E-cadherin adhesion signaling allows luminal surfaces to form at cell–cell adhesion sites in hepatocytic cells. The resulting hepatocytic lumen polarity in turn forces the tilted *x-z* spindle organization as we previously suggested (see Discussion in Lázaro-Diéguez et al., 2013), which then leads to out-of-monolayer divisions in the absence of the elucidated E-cadherin–dependent rescue mechanism.

Discussion

We provide evidence for a mechanical role of E-cadherin mediated cell–cell adhesion in the orientation of cell divisions in monolayered epithelial cells. Key to this role is an adhesion-dependent contractile horizontal actin ring that, in conjunction with polar relaxation, promotes anaphase cell flattening and elongation in the cells' *x-z* dimension. Although previously described E-cadherin–dependent planar spindle orientation mechanisms localize astral MT attachment cues to cell–cell adhesion sites (Lu et al., 2001; Le Borgne et al., 2002; Yamashita et al., 2003; den Elzen et al., 2009; Inaba et al., 2010; Gloerich et al., 2017), the horizontal spindle alignment in anaphase we describe here occurs in response to an adhesion-dependent shape change. Anaphase elongation to accommodate the separating chromatids has previously been described in cells lacking cell–cell adhesion (Brennan et al., 2007; Kiyomitsu and Cheeseman, 2013; Rodrigues et al., 2015). In isolated *Drosophila melanogaster* cells, an equatorial accumulation of myosin II at the site of future cleavage furrow ingression has been linked to anaphase elongation (Hickson et al., 2006). It inevitably decreases circularity in the *x-z* dimension even if cell height is maintained. In agreement with such adhesion-independent cell shape change, we observed a decreased $C_{x\text{-}z}$ index in anaphase compared with metaphase in all cell types and conditions analyzed (unpublished data). However, the $C_{x\text{-}z}$ index decreased to a significantly larger extent under conditions of E-cadherin adhesion (ΔEcad +Dox compared with −Dox) and of high E-cadherin tension, which results from adhesion and linkage to the actin cytoskeleton in control MDCK and Rho-activated WIF-B9 cells. We propose that adhesion-independent anaphase elongation is sufficient to complete mitosis with tilted spindles, whereas additional cell flattening via the subapical myosin II ring causes substrate-parallel spindle alignment. This could result from constraints imposed on the spindle by the cell cortex (Lázaro-Diéguez et al., 2015) or from MT-dependent shape-sensing mechanisms that allow astral MT to equilibrate the spindle in the geometric cell center via pulling or pushing forces that scale with astral MT length (O'Connell and Wang, 2000; Grill and Hyman, 2005; Minc et al., 2011). Such mechanisms are expected to favor smaller β angles in flat cells and are consistent with a larger β angle spread in rounder cells (Minc et al., 2011).

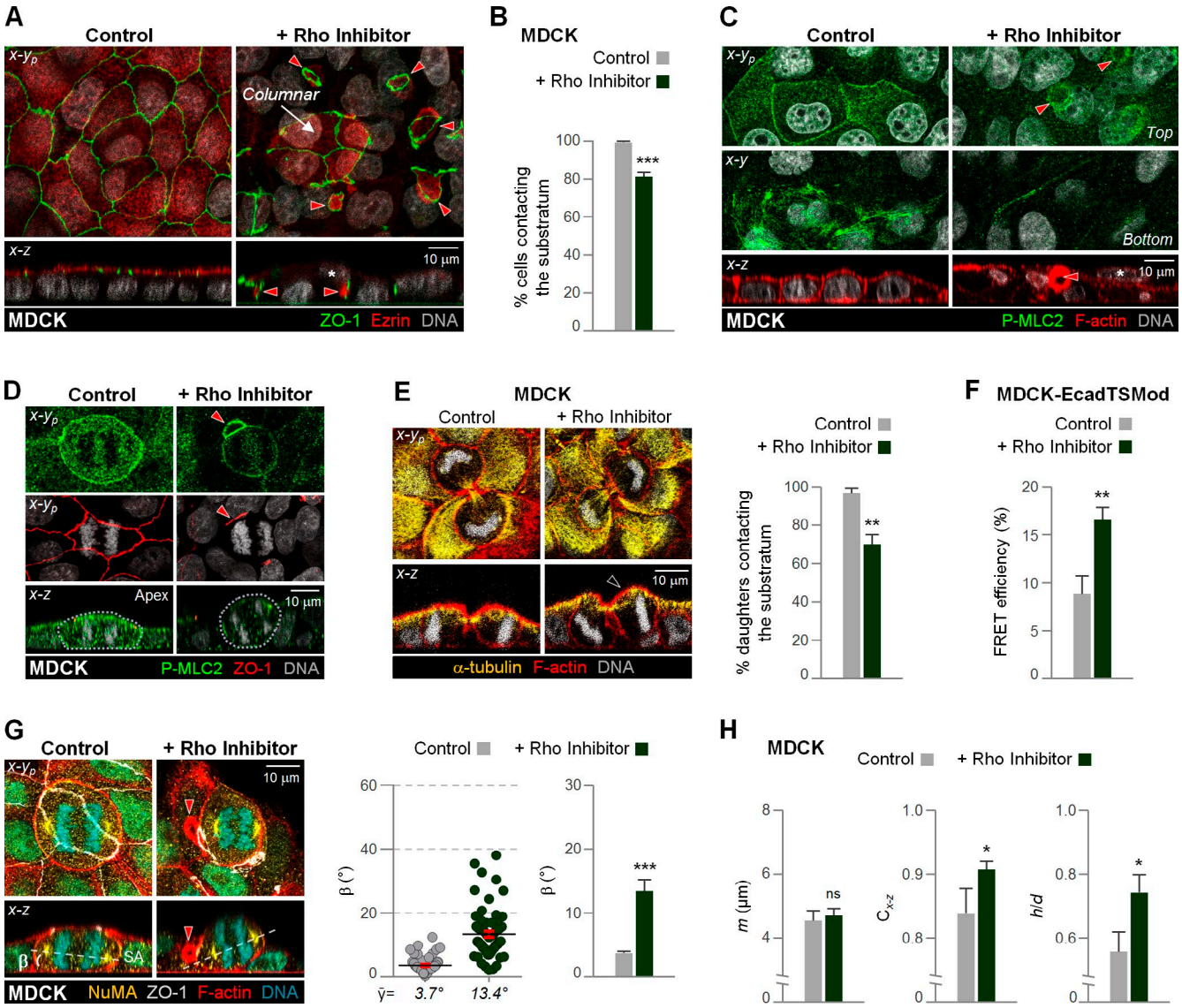

Figure 6. **Rho inhibition promotes a hepatocytic cell division and polarity phenotype in MDCK cells.** (A–H) MDCK cells untreated (control) and treated with a Rho inhibitor were fixed and stained as indicated (A, C–E, and G). Architecture of 2D cultures (A and C), anaphase (D and G), and cytokinesis profiles (E) are shown. Cells not contacting the substratum are denoted by an asterisk in *x-z* views (A and C). (B) The percentage of cells contacting the substratum was quantified. (A) Note the hepatocytic-like pattern of ZO-1 distribution in Rho-inhibited MDCK cells. (E–H) Comparison of the percentage of cytokinesis with both daughter cells contacting the substratum (E), anaphase β angle and *m*, *h/d*, $C_{x\text{-}z}$ values (G and H, respectively), and EcadTSMod FRET efficiency (F). (A, C, D, and G) Red arrowheads show hepatocytic-like lateral lumina. (E) Black arrowhead shows daughter that lost substrate contact. *n* = 20 cells/experiment were analyzed for *N* = 3 independent experiments (B and E–H). Error bars indicate ±SEM (dot graph) and +SD (bar graphs). *, $P \leq 0.05$; **, $P \leq 0.01$; ***, $P \leq 0.001$; ns, nonsignificant, analyzed by *t* test.

It is conceivable that E-cadherin adhesion to surrounding neighbors also reinforces monolayer contact of poorly attached daughter cells during cytokinesis. Yet the adhesion-dependent spindle alignment in anaphase implicates E-cadherin–mediated planar rescue in this step. To our knowledge, this is the first planar spindle rescue mechanism suggested for symmetrical dividing epithelial cells. Previously, a telophase rescue pathway that operates during asymmetric division of neuroblasts has been characterized (Peng et al., 2000; Wang et al., 2006). It is unlikely to play a role in symmetrically dividing epithelial cells, however.

Experimental conditions that disrupt substrate-parallel metaphase spindle orientation in cultured monolayered epithelial cells frequently cause these cells to line multiple rather than a single luminal cavity in 3D cultures (Jaffe et al., 2008; Rodriguez-Fraticelli et al., 2010; Zheng et al., 2010; Tuncay and Ebnet, 2016). Although this is generally taken as evidence that *x-z* spindle orientation defects cause multilayering, the formation of multiple lumina rather than of a solid cell mass in such cultures also implies that multilayering is infrequent even when the incidence of nonparallel metaphase spindles is high. This might be a result of elimination of most cells that lose contact with the basal lamina, but it is also consistent with rescue mechanisms, such as the one characterized here, that prevent out-of-monolayer cytokinesis for cells with misoriented spindles. Remarkably, in addition to rescuing misoriented metaphase spindles, epithelial cells are capable of reintegrating itinerant daughter cells after they have been expelled from

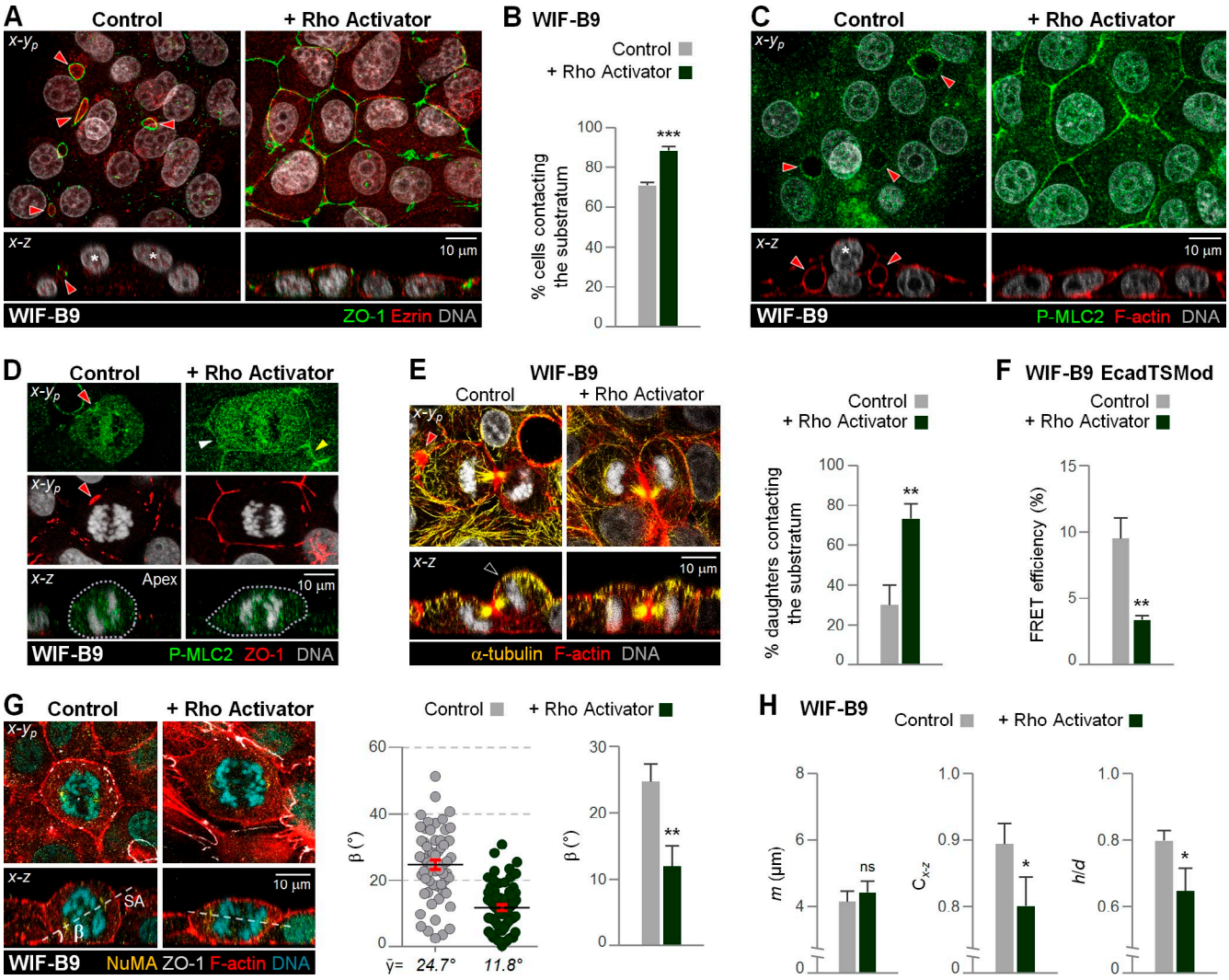

Figure 7. **Rho activation promotes a monolayered cell division and polarity phenotype in WIF-B9 cells.** (A–H) WIF-B9 cells untreated (control) and treated with a Rho activator were fixed and stained as indicated (A, C–E, and G). Architecture of 2D cultures (A and C), anaphase (D and G), and cytokinesis profiles (E) are shown. (A and C) Cells not contacting the substratum are denoted by an asterisk in *x-z* views. The percentage of cells contacting the substratum (B) was quantified. (A) Note the columnar-like pattern of ZO-1 distribution in Rho-activated WIF-B9 cells. (D) White and yellow arrowheads denote junctional-activated myosin II in the mitotic cell and its neighbors, respectively. (E–H) Comparison of the percentage of cytokinesis with both daughter cells contacting the substratum (E), anaphase β angle and *m*, *h/d*, $C_{x\text{-}z}$ values (G and H, respectively), and EcadTSMod FRET efficiency (F). (A and C–E) Red arrowheads show hepatocytic lateral lumina. (E) Black arrowhead shows daughter that lost substrate contact. $n = 20$ cells/experiment were analyzed for $N = 3$ independent experiments (B and E–H). Error bars indicate ±SEM (dot graph) and +SD (bar graphs). *, $P \leq 0.05$; **, $P \leq 0.01$; ***, $P \leq 0.001$; ns, nonsignificant, analyzed by *t* test.

the monolayer by an out-of-plane cytokinesis (Bergstralh et al., 2015), a phenomenon observed in several *Drosophila* cell types and in mouse models of recessive polycystic kidney disease (Nishio et al., 2010). This indicates that monolayered epithelia possess multiple backup mechanisms to prevent cell loss and aberrant tissue organization.

Hepatocytes self-assemble into multilayered, bile-canaliculi–containing spheroids (Tong et al., 1992; Wu et al., 1999; Tostões et al., 2012) and home to blood vessels in vitro (Nahmias et al., 2006), indicating that cell–cell signaling and adhesion mechanisms establish their liver-specific tissue architecture. Out-of-monolayer cell divisions, as we observed in hepatocytic cell cultures, might conceivably contribute to this architecture during recovery from extensive liver damage when adult hepatocytes reenter the cell cycle and divide (Miyaoka et al., 2012). Previous work that characterized hepatocytic division in the *x-y* dimension localized astral MT attachment cues adjacent to the luminal domains that interrupt cell–cell contact sites (Lázaro-Diéguez et al., 2013; Slim et al., 2013). We propose that the cells can accommodate the hepatocyte metaphase spindle only in a quasi-diagonal position, resulting in the *x-z* spindle tilt observed in the hepatocytic cell lines. We presume this to be the case regardless of whether cells possess only a single luminal domain and anchor only one astral MT set to the subluminal cortex (as in Fig. 2 A; Lázaro-Diéguez et al., 2013) or whether cells form luminal domains with multiple neighbors and each astral MT set attaches to cortical cues adjacent to a different luminal domain. In either scenario, cell–cell adhesion forces do not support a substrate-parallel contractile actin ring that would mediate sufficient anaphase cell elongation to decrease the β angle as mitosis progresses, and as a result, an out-of-monolayer cytokinesis ensues. Ongoing developments in

methodology for live-cell imaging of mammalian liver tissue (Porat-Shliom et al., 2016; Meyer et al., 2017) should make it feasible in the future to test this model in vivo.

Materials and methods

Cell lines and culture

MDCK (provided by K. Mostov, University of California, San Francisco, CA) and HepG2 (provided by A. Wolkoff, Albert Einstein College of Medicine, Bronx, NY) cells were grown in DMEM (10-013-CV; Corning) supplemented with 10% FBS (S11050; Atlanta Biologicals) and 2 mM L-alanyl-L-glutamine (25-015-CI; Corning) and 5 mM Hepes buffer. Stable MDCK cell lines coexpressing Par1b-myc (MDCK-Par1b cells) and α-tubulin–RFP were generated from MDCK-Tet-Off cells (Clontech). Control GFP- and LGN-KD-GFP–expressing MDCK clones were provided by Q. Du. (Medical College of Georgia, Augusta, GA). The Dox-dependent ΔE-cadherin MDCK cell line T151 was provided by J. Marrs (Indiana University, Indianapolis, IN). Par1b and ΔE-cadherin expression in MDCK-Tet-Off cells was repressed by 0.1 µg/ml Dox and induced for 3 d after the Dox washout. Stable MDCK cell lines expressing EcadTSMod TFP/YFP FRET biosensor and the corresponding EcadTSMod TFP/YFP plasmid (Borghi et al., 2012) were provided by N. Borghi (Institute Monod, Paris, France). WIF-B9 cells (provided by A. Hubbard, John Hopkins University School of Medicine, Baltimore, MD, and D. Cassio, Universite Paris-Sud, Orsay, France) were grown in modified F-12 Coon's modification medium (F6636; Sigma) supplemented with 5% (vol/vol) FBS (100–106; Gemini), 1% GlutaMAX (35050–061; Life Technologies), 0.5 µg/ml amphotericin, and 5 mM Hepes buffer. WIF-B9 cells were cultured in the presence of 10^{-5} M hypoxanthine, 4×10^{-8} M aminopterin, and 1.6×10^{-6} M thymidine. Cells were maintained at 37°C in a 5% CO_2 (MDCK and HepG2) or 7% (WIF-B9) humidified atmosphere. For culture maintenance, cells were seeded at $\sim 7 \times 10^3$ cells/cm^2 and cultivated up to 2 (MDCK) or 4 d (WIF-B9 and HepG2) before replating. For experiments, MDCK, polarized WIF-B9 cells (10–12 d) and HepG2 cells were plated on water-prewashed uncoated glass in CELL-view (Greiner Bio-One) or MatTek dish chambers at $\sim 1.5 \times 10^5$ cells/cm^2. Cells expressing chloramphenicol acyltransferase and Par1b were obtained by adenovirus transduction in Opti-MEM (Invitrogen) for 1 h with 1–10 plaque-forming units/cell and 24–32 h expression at 37°C in 12–24 h fresh seeded cells. For Rho activation or inhibition, cells were plated in the presence of Rho activator II (CN03; Cytoskeleton) and Rho inhibitor I (cell permeable C3 Transferase; CT04; Cytoskeleton), respectively, at 1 µg/ml and treated for 24 h.

Cell transfections

IQGAP1 siRNA (5′-UGCCAUGGAUGAGAUUGGA-3′; Tanos et al., 2015) was synthetized by Dharmacon. MDCK cells were transfected with RNAi by Amaxa nucleofection (Lonza) and tested 2 or 3 d after plating for protein depletion, then replated at $\sim 1.5 \times 10^5$ cells/cm^2 for analysis after 24 h. WIF-B9 cells were analyzed 24 h after Amaxa nucleofection of EcadTSMod TFP/YFP cDNA.

FRET analysis

The FRET of EcadTSMod TFP and YFP was measured in live cells transiently expressing the EcadTSMod biosensor plasmid (Borghi et al., 2012; WIF-B9) or constitutively (MDCK-EcadTSMod). FRET efficiency was calculated with the acceptor-bleaching FRET module (FRET-AB) of the LAS AF software. For the setup, an HCX PL APO 40×/1.25–0.75 NA oil CS objective was used to obtain pre- and post-bleaching confocal (pinhole, 1 AU; pixel size, 63.1 nm; line mean, 4) *x-y* sections. For the bleaching, a region of interest at the cell cortex was exposed to the 488 argon laser (main power; 80% with 514 nm laser line; 100%, for 20 iterations). The FRET efficiency was evaluated in regions of interest with at least 75% of reduced fluorescence intensity in the acceptor species.

Antibodies and reagents

The following antibodies were used in this study: α-tubulin (rat; ab6160; Abcam), β-catenin (rabbit; C2206; Sigma), E-cadherin [rr1] (Gumbiner and Simons, 1986) provided by Developmental Studies Hybridoma Bank (mouse; DSHB Hybridoma Product rr1), ezrin (rabbit; ab41672, Abcam), GFP (rabbit; ab6556, Abcam), IQGAP1 (mouse; 610611; BD Biosciences), nuclear mitotic apparatus (NuMA; rabbit; ab36999; Abcam), p120 Catenin (mouse; 610134, BD Biosciences), P-MLC2 Thr18/Ser19 (rabbit; 3674; Cell Signaling Technology), and ZO-1 (rat; MABT11; EMD Millipore; or rabbit; 61–7300; ThermoFisher). All fluorescently labeled secondary antibodies were purchased from Jackson ImmunoResearch. DAPI and phalloidin-TRITC and -CF647 were purchased from Sigma and Biotium, respectively. For live imaging experiments, the lumen was stained with BCECF AM or FDA (ThermoFisher) and the DNA with DRAQ5 (Cell Signaling Technology).

Immunofluorescence and confocal microscopy

For immunofluorescence experiments, cells were fixed in 4% PFA in PBS buffer for 20 min at 4°C or room temperature. Alternatively, methanol fixation at −20°C was used for IQGAP1, GFP, and p120 catenin antibodies. PFA-fixed cells were permeabilized in 0.2% Tx100 for 15 min before antibody incubation. F(ab′)$_2$ fragment secondary antibodies coupled to Alexa Fluor 488, Rhodamine Red-X, or Alexa Fluor 647 were used. Chromatin was stained with DAPI or DRAQ5 in fixed or time-lapse experiments, respectively. Microscopy was performed on a TCS SP5 confocal microscope (Leica Microsystems) equipped with a motorized *x-y-z* stage for multiple position finding and with an 8,000 Hz resonant scanner. Cells were imaged using a HCX PL APO 40×/1.25–0.75 oil CS objective on MatTek chambers. Confocal (pinhole, 1 Airy Unit; pixel size, 151.7 nm) *x-y-z* stacks or *x-z* sections were taken from the monolayer. *x-y-z* Projections (*x-y*$_p$) are shown in some panels as indicated. Live cell imaging was performed on MatTek chambers at 37°C in a CO_2–enriched atmosphere in growth medium. The *x-z-t* stacks (pinhole, 3–4 Airy Unit; pixel size, 216.7 nm) were recorded. Images were processed with LAS AF v.2.6.0.7266 (Leica Microsystems) and ImageJ, version 1.51k (National Institutes of Health).

Quantification and statistical analysis

The Circularity index C (4π[area/perimeter^2]) was used to quantify the roundness of a 2D object, corresponding to the cross section of the cell by a plane. The measurements of the circularity ($C_{x\text{-}z}$), the cell dimensions defined by *d*, *h* lengths, the distance between chromatids in anaphase *m*, and the β angle were obtained with the ImageJ tools in *x-z* confocal sections. The location of the spindle poles for β measurements was determined with NuMA antibodies (fixed cells) or α-tubulin-RFP (live cells). We ensured that both spindle poles were contained in the *x-z* confocal plane sections as described in (Lázaro-Diéguez et al., 2015). The mean intensity of E-cadherin was measured at the lateral cell cortex, whereas the P-MLC2 was quantified at the apex in *x-y* or *x-z* confocal sections, respectively. The values were normalized to the highest intensity. To quantify the percentage of cytokinesis with both daughter cells contacting the substratum, cytokinesis profiles were analyzed in the *x-z* dimension. Cell outlines were defined by cortical F-actin staining. To estimate the percentage of cells contacting the substratum, 10 random *x-y* fields of $\sim 6 \times 10^3$ µm^2 were analyzed in the *x-y* and *x-z* dimensions for three independent experiments. For statistical

computation and estimation of significance, we used GraphPad Prism version 6.0 software. Graphs represent mean $\bar{y}$ ± SEM or + SD, as indicated, where (n) represents the number of cells analyzed. Statistical significance was determined using unpaired two-tailed t test for N = three independent experiments. Data distribution was assumed to be normal, but this was not formally tested. Pearson coefficient (r) was applied for correlation analysis.

Online supplemental material

Fig. S1 shows that tilted metaphase spindles in LGN-depleted MDCK cells realign with the substratum during anaphase. Figs. S2 and S3 show adherens and TJs localization during mitosis in MDCK-Par1b and MDCK or WIF-B9 cells, respectively. Fig. S4 shows that E-cadherin binding partner IQGAP is not required for anaphase spindle realignment in LGN-KD cells. Fig. S5 shows the localization of activated myosin II during mitosis in MDCK cells. Video 1 shows that WIF-B9 and HepG2 cells form bilayers in bidimensional cell cultures. Video 2 shows cell divisions out of the monolayer in WIF-B9 cells. Video 3 shows that Par1b overexpression generates bilayers in MDCK cell cultures. Video 4 shows that substitution of E-cadherin for ΔEcad generates bilayers in MDCK cell cultures. Video 5 shows that Rho inhibition promotes hepatocytic-type architecture in MDCK cells. Video 6 shows that Rho activation promotes columnar-type architecture in WIF-B9 cells.

Acknowledgments

We are grateful to Nicolas Borghi for providing the EcadTSMod MDCK cells and plasmids and to Quansheng Du for the LGN-KD MDCK cells.

This work was supported by National Institutes of Health grant R01 DK064842 to A. Müsch.

The authors declare no competing financial interests.

Author contributions: F. Lázaro-Diéguez performed experiments, analyzed data, and generated the figures. F. Lázaro-Diéguez and A. Müsch designed the study and wrote the manuscript.

Submitted: 19 August 2016
Revised: 1 June 2017
Accepted: 8 August 2017

References

Bañón-Rodríguez, I., M. Gálvez-Santisteban, S. Vergarajauregui, M. Bosch, A. Borreguero-Pascual, and F. Martín-Belmonte. 2014. EGFR controls IQGAP basolateral membrane localization and mitotic spindle orientation during epithelial morphogenesis. *EMBO J.* 33:129–145. http://dx.doi.org/10.1002/embj.201385946

Bartles, J.R., and A.L. Hubbard. 1986. Preservation of hepatocyte plasma membrane domains during cell division in situ in regenerating rat liver. *Dev. Biol.* 118:286–295. http://dx.doi.org/10.1016/0012-1606(86)90095-3

Bell, C.C., D.F. Hendriks, S.M. Moro, E. Ellis, J. Walsh, A. Renblom, L. Fredriksson Puigvert, A.C. Dankers, F. Jacobs, J. Snoeys, et al. 2016. Characterization of primary human hepatocyte spheroids as a model system for drug-induced liver injury, liver function and disease. *Sci. Rep.* 6:25187. http://dx.doi.org/10.1038/srep25187

Bergstralh, D.T., and D. St Johnston. 2014. Spindle orientation: What if it goes wrong? *Semin. Cell Dev. Biol.* 34:140–145. http://dx.doi.org/10.1016/j.semcdb.2014.06.014

Bergstralh, D.T., H.E. Lovegrove, and D. St Johnston. 2015. Lateral adhesion drives reintegration of misplaced cells into epithelial monolayers. *Nat. Cell Biol.* 17:1497–1503. http://dx.doi.org/10.1038/ncb3248

Borghi, N., M. Sorokina, O.G. Shcherbakova, W.I. Weis, B.L. Pruitt, W.J. Nelson, and A.R. Dunn. 2012. E-cadherin is under constitutive actomyosin-generated tension that is increased at cell-cell contacts upon externally applied stretch. *Proc. Natl. Acad. Sci. USA.* 109:12568–12573. (published erratum appears in *Proc. Natl. Acad. Sci. USA.* 109:19034) PubMed https://doi.org/10.1073/pnas.1204390109

Brennan, I.M., U. Peters, T.M. Kapoor, and A.F. Straight. 2007. Polo-like kinase controls vertebrate spindle elongation and cytokinesis. *PLoS One.* 2:e409. http://dx.doi.org/10.1371/journal.pone.0000409

Cadart, C., E. Zlotek-Zlotkiewicz, M. Le Berre, M. Piel, and H.K. Matthews. 2014. Exploring the function of cell shape and size during mitosis. *Dev. Cell.* 29:159–169. http://dx.doi.org/10.1016/j.devcel.2014.04.009

Cohen, D., P.J. Brennwald, E. Rodriguez-Boulan, and A. Müsch. 2004. Mammalian PAR-1 determines epithelial lumen polarity by organizing the microtubule cytoskeleton. *J. Cell Biol.* 164:717–727. http://dx.doi.org/10.1083/jcb.200308104

Decaens, C., M. Durand, B. Grosse, and D. Cassio. 2008. Which in vitro models could be best used to study hepatocyte polarity? *Biol. Cell.* 100:387–398. http://dx.doi.org/10.1042/BC20070127

den Elzen, N., C.V. Buttery, M.P. Maddugoda, G. Ren, and A.S. Yap. 2009. Cadherin adhesion receptors orient the mitotic spindle during symmetric cell division in mammalian epithelia. *Mol. Biol. Cell.* 20:3740–3750. http://dx.doi.org/10.1091/mbc.E09-01-0023

Gerber, M.A., and S.N. Thung. 1987. Histology of the liver. *Am. J. Surg. Pathol.* 11:709–722. http://dx.doi.org/10.1097/00000478-198709000-00007

Gissen, P., and I.M. Arias. 2015. Structural and functional hepatocyte polarity and liver disease. *J. Hepatol.* 63:1023–1037. http://dx.doi.org/10.1016/j.jhep.2015.06.015

Gloerich, M., J.M. Bianchini, K.A. Siemers, D.J. Cohen, and W.J. Nelson. 2017. Cell division orientation is coupled to cell-cell adhesion by the E-cadherin/LGN complex. *Nat. Commun.* 8:13996. http://dx.doi.org/10.1038/ncomms13996

Grill, S.W., and A.A. Hyman. 2005. Spindle positioning by cortical pulling forces. *Dev. Cell.* 8:461–465. http://dx.doi.org/10.1016/j.devcel.2005.03.014

Gumbiner, B., and K. Simons. 1986. A functional assay for proteins involved in establishing an epithelial occluding barrier: identification of a uvomorulin-like polypeptide. *J. Cell Biol.* 102:457–468. http://dx.doi.org/10.1083/jcb.102.2.457

Hickson, G.R., A. Echard, and P.H. O'Farrell. 2006. Rho-kinase controls cell shape changes during cytokinesis. *Curr. Biol.* 16:359–370. http://dx.doi.org/10.1016/j.cub.2005.12.043

Hoekstra, D., M.M. Zegers, and S.C. van Ijzendoorn. 1999. Membrane flow, lipid sorting and cell polarity in HepG2 cells: role of a subapical compartment. *Biochem. Soc. Trans.* 27:422–428. http://dx.doi.org/10.1042/bst0270422

Ihara, A., H. Koizumi, R. Hashizume, and T. Uchikoshi. 1996. Expression of epithelial cadherin and alpha- and beta-catenins in nontumoral livers and hepatocellular carcinomas. *Hepatology.* 23:1441–1447.

Ihrke, G., E.B. Neufeld, T. Meads, M.R. Shanks, D. Cassio, M. Laurent, T.A. Schroer, R.E. Pagano, and A.L. Hubbard. 1993. WIF-B cells: An in vitro model for studies of hepatocyte polarity. *J. Cell Biol.* 123:1761–1775. http://dx.doi.org/10.1083/jcb.123.6.1761

Inaba, M., H. Yuan, V. Salzmann, M.T. Fuller, and Y.M. Yamashita. 2010. E-cadherin is required for centrosome and spindle orientation in Drosophila male germline stem cells. *PLoS One*. 5:e12473. http://dx.doi.org/10.1371/journal.pone.0012473

Jaffe, A.B., N. Kaji, J. Durgan, and A. Hall. 2008. Cdc42 controls spindle orientation to position the apical surface during epithelial morphogenesis. *J. Cell Biol.* 183:625–633. http://dx.doi.org/10.1083/jcb.200807121

Jüschke, C., Y. Xie, M.P. Postiglione, and J.A. Knoblich. 2014. Analysis and modeling of mitotic spindle orientations in three dimensions. *Proc. Natl. Acad. Sci. USA.* 111:1014–1019. http://dx.doi.org/10.1073/pnas.1314984111

Kelm, J.M., N.E. Timmins, C.J. Brown, M. Fussenegger, and L.K. Nielsen. 2003. Method for generation of homogeneous multicellular tumor spheroids applicable to a wide variety of cell types. *Biotechnol. Bioeng.* 83:173–180. http://dx.doi.org/10.1002/bit.10655

Kiyomitsu, T., and I.M. Cheeseman. 2013. Cortical dynein and asymmetric membrane elongation coordinately position the spindle in anaphase. *Cell.* 154:391–402. (published erratum appears in *Cell.* 154:1401) http://dx.doi.org/10.1016/j.cell.2013.06.010

Kotadia, S., E. Montembault, W. Sullivan, and A. Royou. 2012. Cell elongation is an adaptive response for clearing long chromatid arms from the cleavage plane. *J. Cell Biol.* 199:745–753. http://dx.doi.org/10.1083/jcb.201208041

Kotak, S., C. Busso, and P. Gönczy. 2012. Cortical dynein is critical for proper spindle positioning in human cells. *J. Cell Biol.* 199:97–110. http://dx.doi.org/10.1083/jcb.201203166

Lázaro-Diéguez, F., D. Cohen, D. Fernandez, L. Hodgson, S.C. van Ijzendoorn, and A. Müsch. 2013. Par1b links lumen polarity with LGN-NuMA

positioning for distinct epithelial cell division phenotypes. *J. Cell Biol.* 203:251–264. http://dx.doi.org/10.1083/jcb.201303013

Lázaro-Diéguez, F., I. Ispolatov, and A. Müsch. 2015. Cell shape impacts on the positioning of the mitotic spindle with respect to the substratum. *Mol. Biol. Cell.* 26:1286–1295. http://dx.doi.org/10.1091/mbc.E14-08-1330

Le Borgne, R., Y. Bellaïche, and F. Schweisguth. 2002. Drosophila E-cadherin regulates the orientation of asymmetric cell division in the sensory organ lineage. *Curr. Biol.* 12:95–104. http://dx.doi.org/10.1016/S0960-9822(01)00648-0

Lechler, T., and E. Fuchs. 2005. Asymmetric cell divisions promote stratification and differentiation of mammalian skin. *Nature.* 437:275–280. http://dx.doi.org/10.1038/nature03922

Lu, B., F. Roegiers, L.Y. Jan, and Y.N. Jan. 2001. Adherens junctions inhibit asymmetric division in the Drosophila epithelium. *Nature*. 409:522–525. http://dx.doi.org/10.1038/35054077

Maier, B., M. Kirsch, S. Anderhub, H. Zentgraf, and A. Krämer. 2013. The novel actin/focal adhesion-associated protein MISP is involved in mitotic spindle positioning in human cells. *Cell Cycle.* 12:1457–1471. http://dx.doi.org/10.4161/cc.24602

Meng, W., and M. Takeichi. 2009. Adherens junction: Molecular architecture and regulation. *Cold Spring Harb. Perspect. Biol.* 1:a002899. http://dx.doi.org/10.1101/cshperspect.a002899

Meyer, K., O. Ostrenko, G. Bourantas, H. Morales-Navarrete, N. Porat-Shliom, F. Segovia-Miranda, H. Nonaka, A. Ghaemi, J.M. Verbavatz, L. Brusch, et al.2017. A predictive 3D multi-scale model of biliary fluid dynamics in the liver lobule. Cell Syst.http://dx.doi.org/10.1016/j.cels.2017.02.008

Minc, N., D. Burgess, and F. Chang. 2011. Influence of cell geometry on division-plane positioning. *Cell.* 144:414–426. http://dx.doi.org/10.1016/j.cell.2011.01.016

Miyaoka, Y., K. Ebato, H. Kato, S. Arakawa, S. Shimizu, and A. Miyajima. 2012. Hypertrophy and unconventional cell division of hepatocytes underlie liver regeneration. *Curr. Biol.* 22:1166–1175. http://dx.doi.org/10.1016/j.cub.2012.05.016

Nahmias, Y., R.E. Schwartz, W.S. Hu, C.M. Verfaillie, and D.J. Odde. 2006. Endothelium-mediated hepatocyte recruitment in the establishment of liver-like tissue in vitro. *Tissue Eng.* 12:1627–1638. http://dx.doi.org/10.1089/ten.2006.12.1627

Nishio, S., X. Tian, A.R. Gallagher, Z. Yu, V. Patel, P. Igarashi, and S. Somlo. 2010. Loss of oriented cell division does not initiate cyst formation. *J. Am. Soc. Nephrol.* 21:295–302. http://dx.doi.org/10.1681/ASN.2009060603

O'Connell, C.B., and Y.L. Wang. 2000. Mammalian spindle orientation and position respond to changes in cell shape in a dynein-dependent fashion. *Mol. Biol. Cell.* 11:1765–1774. http://dx.doi.org/10.1091/mbc.11.5.1765

Peng, C.Y., L. Manning, R. Albertson, and C.Q. Doe. 2000. The tumour-suppressor genes lgl and dlg regulate basal protein targeting in *Drosophila* neuroblasts. *Nature.* 408:596–600. http://dx.doi.org/10.1038/35046094

Polyakov, O., B. He, M. Swan, J.W. Shaevitz, M. Kaschube, and E. Wieschaus. 2014. Passive mechanical forces control cell-shape change during *Drosophila* ventral furrow formation. *Biophys. J.* 107:998–1010. http://dx.doi.org/10.1016/j.bpj.2014.07.013

Porat-Shliom, N., A.J. Tietgens, C.M. Van Itallie, L. Vitale-Cross, M. Jarnik, O.J. Harding, J.M. Anderson, J.S. Gutkind, R. Weigert, and I.M. Arias. 2016. Liver kinase B1 regulates hepatocellular tight junction distribution and function in vivo. *Hepatology.* 64:1317–1329. http://dx.doi.org/10.1002/hep.28724

Priya, R., G.A. Gomez, S. Budnar, S. Verma, H.L. Cox, N.A. Hamilton, and A.S. Yap. 2015. Feedback regulation through myosin II confers robustness on RhoA signalling at E-cadherin junctions. *Nat. Cell Biol.* 17:1282–1293. http://dx.doi.org/10.1038/ncb3239

Ragkousi, K., and M.C. Gibson. 2014. Cell division and the maintenance of epithelial order. *J. Cell Biol.* 207:181–188. http://dx.doi.org/10.1083/jcb.201408044

Reinsch, S., and E. Karsenti. 1994. Orientation of spindle axis and distribution of plasma membrane proteins during cell division in polarized MDCKII cells. *J. Cell Biol.* 126:1509–1526. http://dx.doi.org/10.1083/jcb.126.6.1509

Rodrigues, N.T., S. Lekomtsev, S. Jananji, J. Kriston-Vizi, G.R. Hickson, and B. Baum. 2015. Kinetochore-localized PP1-Sds22 couples chromosome segregation to polar relaxation. *Nature.* 524:489–492. http://dx.doi.org/10.1038/nature14496

Rodriguez-Fraticelli, A.E., S. Vergarajauregui, D.J. Eastburn, A. Datta, M.A. Alonso, K. Mostov, and F. Martín-Belmonte. 2010. The Cdc42 GEF Intersectin 2 controls mitotic spindle orientation to form the lumen during epithelial morphogenesis. *J. Cell Biol.* 189:725–738. http://dx.doi.org/10.1083/jcb.201002047

Rosin-Arbesfeld, R., G. Ihrke, and M. Bienz. 2001. Actin-dependent membrane association of the APC tumour suppressor in polarized mammalian epithelial cells. *EMBO J.* 20:5929–5939. http://dx.doi.org/10.1093/emboj/20.21.5929

Shewan, A.M., M. Maddugoda, A. Kraemer, S.J. Stehbens, S. Verma, E.M. Kovacs, and A.S. Yap. 2005. Myosin 2 is a key Rho kinase target necessary for the local concentration of E-cadherin at cell-cell contacts. *Mol. Biol. Cell.* 16:4531–4542. http://dx.doi.org/10.1091/mbc.E05-04-0330

Siller, K.H., and C.Q. Doe. 2009. Spindle orientation during asymmetric cell division. *Nat. Cell Biol.* 11:365–374. http://dx.doi.org/10.1038/ncb0409-365

Slim, C.L., F. Lázaro-Diéguez, M. Bijlard, M.J. Toussaint, A. de Bruin, Q. Du, A. Müsch, and S.C. van Ijzendoorn. 2013. Par1b induces asymmetric inheritance of plasma membrane domains via LGN-dependent mitotic spindle orientation in proliferating hepatocytes. *PLoS Biol.* 11:e1001739. http://dx.doi.org/10.1371/journal.pbio.1001739

Tanos, B.E., A.E. Perez Bay, S. Salvarezza, I. Vivanco, I. Mellinghoff, M. Osman, D.B. Sacks, and E. Rodriguez-Boulan. 2015. IQGAP1 controls tight junction formation through differential regulation of claudin recruitment. *J. Cell Sci.* 128:853–862. http://dx.doi.org/10.1242/jcs.118703

Tong, J.Z., P. De Lagausie, V. Furlan, T. Cresteil, O. Bernard, and F. Alvarez. 1992. Long-term culture of adult rat hepatocyte spheroids. *Exp. Cell Res.* 200:326–332. http://dx.doi.org/10.1016/0014-4827(92)90179-C

Tostões, R.M., S.B. Leite, M. Serra, J. Jensen, P. Björquist, M.J. Carrondo, C. Brito, and P.M. Alves. 2012. Human liver cell spheroids in extended perfusion bioreactor culture for repeated-dose drug testing. *Hepatology.* 55:1227–1236. http://dx.doi.org/10.1002/hep.24760

Toyoshima, F., S. Matsumura, H. Morimoto, M. Mitsushima, and E. Nishida. 2007. PtdIns(3,4,5)P3 regulates spindle orientation in adherent cells. *Dev. Cell.* 13:796–811. http://dx.doi.org/10.1016/j.devcel.2007.10.014

Treyer, A., and A. Müsch. 2013. Hepatocyte polarity. *Compr. Physiol.* 3:243–287.

Troxell, M.L., D.J. Loftus, W.J. Nelson, and J.A. Marrs. 2001. Mutant cadherin affects epithelial morphogenesis and invasion, but not transformation. *J. Cell Sci.* 114:1237–1246.

Tuncay, H., and K. Ebnet. 2016. Cell adhesion molecule control of planar spindle orientation. *Cell. Mol. Life Sci.* 73:1195–1207. http://dx.doi.org/10.1007/s00018-015-2116-7

Wang, H., Y. Cai, W. Chia, and X. Yang. 2006. *Drosophila* homologs of mammalian TNF/TNFR-related molecules regulate segregation of Miranda/Prospero in neuroblasts. *EMBO J.* 25:5783–5793. http://dx.doi.org/10.1038/sj.emboj.7601461

Williams, S.E., and E. Fuchs. 2013. Oriented divisions, fate decisions. *Curr. Opin. Cell Biol.* 25:749–758. http://dx.doi.org/10.1016/j.ceb.2013.08.003

Woodard, G.E., N.N. Huang, H. Cho, T. Miki, G.G. Tall, and J.H. Kehrl. 2010. Ric-8A and Gi alpha recruit LGN, NuMA, and dynein to the cell cortex to help orient the mitotic spindle. *Mol. Cell. Biol.* 30:3519–3530. http://dx.doi.org/10.1128/MCB.00394-10

Wu, F.J., J.R. Friend, R.P. Remmel, F.B. Cerra, and W.S. Hu. 1999. Enhanced cytochrome P450 IA1 activity of self-assembled rat hepatocyte spheroids. *Cell Transplant.* 8:233–246. http://dx.doi.org/10.1177/096368979900800304

Yamashita, Y.M., D.L. Jones, and M.T. Fuller. 2003. Orientation of asymmetric stem cell division by the APC tumor suppressor and centrosome. *Science*. 301:1547–1550. http://dx.doi.org/10.1126/science.1087795

Yonemura, S. 2011. Cadherin-actin interactions at adherens junctions. *Curr. Opin. Cell Biol.* 23:515–522. http://dx.doi.org/10.1016/j.ceb.2011.07.001

Zheng, Z., H. Zhu, Q. Wan, J. Liu, Z. Xiao, D.P. Siderovski, and Q. Du. 2010. LGN regulates mitotic spindle orientation during epithelial morphogenesis. *J. Cell Biol.* 189:275–288. http://dx.doi.org/10.1083/jcb.200910021